Estimation of Gait Kinematics and Kinetics from Inertial Sensor Data Using Optimal Control of Musculoskeletal Models

Eva Dorschky, Marlies Nitschke, Ann-Kristin Seifer, Antonie J. van den Bogert, Bjoern M. Eskofier

PII: S0021-9290(19)30484-1
DOI: https://doi.org/10.1016/j.jbiomech.2019.07.022
Reference: BM 9278

To appear in: *Journal of Biomechanics*

Received Date: 31 January 2019
Accepted Date: 18 July 2019

Please cite this article as: E. Dorschky, M. Nitschke, A-K. Seifer, A.J. van den Bogert, B.M. Eskofier, Estimation of Gait Kinematics and Kinetics from Inertial Sensor Data Using Optimal Control of Musculoskeletal Models, *Journal of Biomechanics* (2019), doi: https://doi.org/10.1016/j.jbiomech.2019.07.022

Estimation of Gait Kinematics and Kinetics from Inertial Sensor Data Using Optimal Control of Musculoskeletal Models

Eva Dorschky[a], Marlies Nitschke[a], Ann-Kristin Seifer[a], Antonie J. van den Bogert[b], Bjoern M. Eskofier[a]

[a] *Machine Learning and Data Analytics Lab, University of Erlangen-Nürnberg (FAU), Germany*
[b] *Mechanical Engineering Department, Cleveland State University, USA*

Keywords: gait analysis, inertial sensors, motion capturing, optimal control

Resubmission of Manuscript BM-D-19-00090R2

Word Count (Introduction through Acknowledgements): 3981
Word Count (Introduction through Appendices): 4342

Corresponding Author

Eva Dorschky, M.Sc.
Machine Learning and Data Analytics Lab
Department of Computer Science
Friedrich-Alexander-Universität Erlangen-Nürnberg (FAU)
Carl-Thiersch-Strasse 2b, 91052 Erlangen, Germany
Phone: +49 9131 85-27890
Mail: eva.dorschky@fau.de

Abstract

Inertial sensing enables field studies of human movement and ambulant assessment of patients. However, the challenge is to obtain a comprehensive analysis from low-quality data and sparse measurements. In this paper, we present a method to estimate gait kinematics and kinetics directly from raw inertial sensor data performing a single dynamic optimization. We formulated an optimal control problem to track accelerometer and gyroscope data with a planar musculoskeletal model. In addition, we minimized muscular effort to ensure a unique solution and to prevent the model from tracking noisy measurements too closely. For evaluation, we recorded data of ten subjects walking and running at six different speeds using seven inertial measurement units (IMUs). Results were compared to a conventional analysis using optical motion capture and a force plate. High correlations were achieved for gait kinematics ($\rho \geq 0.93$) and kinetics ($\rho \geq 0.90$). In contrast to existing IMU processing methods, a dynamically consistent simulation was obtained and we were able to estimate running kinetics. Besides kinematics and kinetics, further metrics such as muscle activations and metabolic cost can be directly obtained from simulated model movements. In summary, the method is insensitive to sensor noise and drift and provides a detailed analysis solely based on inertial sensor data.

1. Introduction

Human gait gives insight into human health and motor control. Gait analysis is commonly used to support medical diagnosis, monitoring the rehabilitation process of patients and quantifying the performance of athletes. In a gold-standard gait laboratory, camera-based systems and force plates are installed to compute gait kinematics and kinetics. These systems are expensive and restricted to a limited field of view in time and space. It is often desired to carry out a high quality analysis under non-laboratory conditions, e.g. for the ambulant assessment of patients or for analyzing athletes' performance on the field.

Body sensor networks with integrated inertial measurement units (IMUs) such as Xsens MVN (Xsens Technologies BV, Enschede, NL) promise a quantitative movement analysis in unconstrained environments. However, inertial measurement units (IMUs) suffer from measurement noise and drifting biases making an integration-based analysis difficult (Sabatini et al., 2015). Moreover, inertial sensors provide only kinematic data. Other sensor modalities, e.g. pressure insoles or electromyography (EMG), can be used to estimate additional parameters like joint loads or muscle activity patterns. However, the usage of a large number of sensors increases cost and inhibits natural movements. Overall, two problems need to be addressed: (1) sensor noise and drift and (2) a comprehensive analysis based on a limited number of sensors and sensor modalities.

Filtering- and global optimization-based approaches have been proposed to cope with sensor noise and drift. For example, Roetenberg et al. (2005) presented an extended Kalman filter using sensor fusion. Using kinematic body models and external contacts, errors in the predicted segment positions and orientations could be corrected (Roetenberg et al., 2009). Besides filtering, optimization-based techniques were proposed to estimate relative positions and orientations of body segments. Koning et al. (2013) solved a global optimization problem to simulate a biomechanical model. During optimization, the difference between orientations of the model segments and orientations computed by sensor fusion of IMU data was minimized. Hence, errors in orientation estimation were directly incorporated into the optimization. Kok et al. (2014) estimated the relative position and orientation of each body segment by solving an maximum-a-posteriori optimization problem. They modeled accelerometer noise and gyroscope bias using a Gaussian distribution and included biomechanical constraints to obtain a drift-free estimation of joint angles.

All the above described methods provide only gait kinematics. Kinetic analysis is also of interest, which relates to the second above-mentioned challenge. On the one hand, additional sensors like instrumented force shoes (Liedtke et al., 2007; Liu et al., 2010; Schepers et al., 2009) could be used. On the other hand, methods have been proposed to estimate gait kinetics based only on IMU data (reviewed by Ancillao et al. (2018)). Machine learning approaches show promising results for estimating specific gait parameters (Hannink et al., 2016; Wouda et al., 2018). However, the collection of representative training data is time-consuming and sometimes infeasible. Unlike data-driven approaches, musculoskeletal simulation yields interpretable results providing insights into muscular control and mechanical characteristics of movement. To date, Karatsidis et al. (2018) presented the most extensive kinematic and kinetic gait

analysis based on IMUs and musculoskeletal modeling. They obtained segment positions and orientations from the Xsens system with 17 IMUs and computed kinematics by constrained optimization. Afterwards, they solved a static optimization problem to obtain the muscle reaction forces for the given computed motion trajectory by minimizing muscle activity subject to dynamic equilibrium constraints. Joint moments and ground reaction forces (GRFs) were estimated using inverse dynamics. Karatsidis et al. (2018) evaluated their method on walking at different speeds. It would be of interest to know how their method performs on highly dynamic movements like running, as they derived muscle forces based on static optimization. However, static optimization cannot account for time-dependent interactions like muscle activation-deactivation dynamics and elastic energy storage in the tendons (Prilutsky and Zatsiorsky, 2002). Furthermore, different tools were sequentially used including the Xsens and Anybody system which limits the applicability of the procedure to these commercial systems.

In contrast, we propose a dynamic optimization which yields a dynamically consistent simulation. Moreover, we would like to reduce the number of necessary tools, processing steps and IMUs to make the analysis practical for clinical and use in sports.

Our goal is to estimate gait kinematics and kinetics directly from raw inertial sensor data performing one global dynamic optimization. Therefore, we formulated an optimal control problem to find movement and muscular control trajectories of gait cycles. The method is based on van den Bogert et al. (2011) and was already applied for estimating knee joint loads from noisy video data (Heinrich et al., 2014). Our contribution is the extension and evaluation of the optimal control simulation to estimate sagittal kinematics and kinetics of the lower limbs from IMU data. First, we describe the planar musculoskeletal model in Sec. 2.1 and virtual sensor model in Sec. 2.2. In Sec. 2.3, the optimal control problem is formulated. We conducted an evaluation study using seven IMUs placed on the lower limbs and an optical motion capturing system including one force plate as the gold standard for purposes of comparison. In total, we recorded ten healthy male subjects walking and running overground at three different speeds each (see Sec. 2.4).

2. Methods

2.1. Musculoskeletal Model and Dynamics

The planar musculoskeletal model consisted of seven rigid segments, one segment representing the head, arms and torso denoted as trunk, and three segments for each lower extremity (see Fig. 1). The segment masses, lengths, center of mass locations, and moments of inertia were estimated based on subject heights and body masses using the regression equations of Winter (2009). In total, the model had nine kinematic degrees of freedom summarized as generalized coordinates in vector $\mathbf{q} := \left[\mathbf{p}^G_{\text{trunk}}, \theta_{\text{trunk}|G}, \theta_{\text{thigh\_r}|\text{trunk}}, \theta_{\text{shank\_r}|\text{thigh\_r}}, \theta_{\text{foot\_r}|\text{shank\_r}}, \theta_{\text{thigh\_l}|\text{trunk}}, \theta_{\text{shank\_l}|\text{thigh\_l}}, \theta_{\text{foot\_l}|\text{shank\_l}}\right]^T$ comprising the 2D position of the trunk in global frame G, the sagittal orientation of the trunk relative to G, and the right and left leg joint angles in sagittal plane (see Fig. 1). We defined the time derivative of $\mathbf{q}$ as generalized velocities $\mathbf{v}$.

The model was actuated by 16 muscles, eight for each lower extremity as shown in Fig. 1. Each muscle was modeled as three-element Hill-type model. The muscle contraction and activation dynamics are explained in van den Bogert et al. (2011). The state of each muscle was described by the length of the contractive element L_{CE} and its activation α. In addition, we defined two contact points at each foot (heel and toe) to model the foot-contact interaction. Each contact point introduced four state variables: the global position of the contact point $\left[c_x^G, c_y^G\right]^T$ and the global force exerted by the ground on the contact point $\left[F_{c_x}^G, F_{c_y}^G\right]^T$. A detailed formulation of contact dynamics can be found in Appendix A. Altogether, the model's state was represented by the state vector:

$$\mathbf{x} := \begin{bmatrix} \mathbf{q} & \text{nine generalized coordinates} \\ \mathbf{v} & \text{nine generalized velocities} \\ \mathbf{L_{CE}} & \text{16 contractile elements lengths} \\ \alpha & \text{16 muscle activations} \\ \left[c_{x,1}, c_{y,1}, F_{c_{x,1}}, F_{c_{y,1}}\right]^T & \text{global position and force at 1st contact point} \\ & \vdots \\ \left[c_{x,4}, c_{y,4}, F_{c_{x,4}}, F_{c_{y,4}}\right]^T & \text{global position and force at last contact point} \end{bmatrix}. \tag{1}$$

The model was driven by the control vector $\mathbf{u}$ comprising the 16 neural excitations of the muscles. The system dynamics were implicitly formulated as function of $\mathbf{x}$, $\dot{\mathbf{x}}$, and $\mathbf{u}$:

$$\mathbf{f}(\mathbf{x}, \dot{\mathbf{x}}, \mathbf{u}) = \mathbf{0}. \tag{2}$$

The function $\mathbf{f}()$ consisted of nine identities $\mathbf{v} - \dot{\mathbf{q}} = \mathbf{0}$, 16 muscle contraction and 16 activation dynamics equations (van den Bogert et al., 2011), 16 contact equations, and nine multi-body equations of motion (see Appendix A). The system dynamics $\mathbf{f}()$ were twice differentiable with respect to $\mathbf{x}$, $\dot{\mathbf{x}}$, and $\mathbf{u}$. This made it possible to use a gradient-based optimal control method in Sec. 2.3.

2.2. Virtual Sensor Model

We tracked accelerometer and gyroscope data with the planar musculoskeletal model in the optimal control simulation in Sec. 2.3. Therefore, we placed virtual sensors at the musculoskeletal model producing comparable accelerometer and gyroscope signals as would be measured by real sensors (see Fig 2). We assumed that the IMUs were rigidly attached to the body segments $\mathrm{s} \in \mathscr{S} = \{\text{trunk}, \text{thigh\_r}, \text{shank\_r}, \text{foot\_r}, \text{thigh\_l}, \text{shank\_l}, \text{foot\_l}\}$ at a known position $\mathbf{p}^{B_\mathrm{s}}$ in the body-segment coordinate system B_s. Additionally, we ensured that the sensor axes were aligned with B_s. The gyroscope signal in the sagittal-plane ω_s was equal to the angular velocity of the corresponding body segment with

respect to global frame G and was calculated from the generalized velocities $\mathbf{v}$:

$$\omega_{\text{trunk}} := \dot{\theta}_{\text{trunk}|G}, \tag{3}$$

$$\omega_{\text{thigh\_r/l}} := \dot{\theta}_{\text{thigh\_r/l}|G} = \dot{\theta}_{\text{thigh\_r/l}|\text{trunk}} + \dot{\theta}_{\text{trunk}|G}, \tag{4}$$

$$\omega_{\text{shank\_r/l}} := \dot{\theta}_{\text{shank\_r/l}|G} = \dot{\theta}_{\text{shank\_r/l}|\text{thigh\_r/l}} + \dot{\theta}_{\text{thigh\_r/l}|G}, \tag{5}$$

$$\omega_{\text{foot\_r/l}} := \dot{\theta}_{\text{foot\_r/l}|G} = \dot{\theta}_{\text{foot\_r/l}|\text{shank\_r/l}} + \dot{\theta}_{\text{shank\_r/l}|G}. \tag{6}$$

An equation for the accelerometer signal $\mathbf{a}_s = [a_{x,s}, a_{y,s}]^T$ that would be measured at a body segment is given in van den Bogert et al. (1996). In 2D, the formula can be simplified to

$$\mathbf{a}_s := \mathbf{R}^{B_\text{s}G}\left(\mathbf{a}^G_{G|B_\text{s}} - \mathbf{g}\right) + \begin{bmatrix} -\omega_\text{s}^2 & -\dot{\omega}_\text{s} \\ \dot{\omega}_\text{s} & -\omega_\text{s}^2 \end{bmatrix} \mathbf{p}^{B_\text{s}}, \tag{7}$$

where $\mathbf{R}^{B_\text{s}G}$ is the transformation matrix from global frame to B_s, $\mathbf{a}^G_{G|B_\text{s}}$ is the acceleration of the segment origin relative to G (in G coordinates) and $\mathbf{g} = \left[0, -9.81\,\text{m/s}^2\right]^T$. We used Autolev 4.1 to generate a symbolic expression of Eq. 7 as a function of the kinematic states $\mathbf{q}$, $\mathbf{v}$, $\dot{\mathbf{v}}$ and sensor position $\mathbf{p}^{B_\text{s}}$. The time derivative $\dot{\mathbf{v}}$ was estimated using finite difference approximation.

2.3. Optimal Control Problem

The goal was to find the model states $\mathbf{x}(t)$ and controls $\mathbf{u}(t)$ during one gait cycle of duration T, such that the simulated acceleration and angular velocity corresponded to the measured signals without sensor noise. This was done by solving an optimal control problem following van den Bogert et al. (2011):

$$\begin{aligned} \underset{\mathbf{x}(t),\mathbf{u}(t)}{\text{minimize}} \quad & J(\mathbf{x}(t),\mathbf{u}(t)) \\ \text{subject to} \quad & \mathbf{x}_\text{L} \le \mathbf{x} \le \mathbf{x}_\text{U} \\ & \mathbf{u}_\text{L} \le \mathbf{u} \le \mathbf{u}_\text{U} \\ & f(\mathbf{x}(t), \dot{\mathbf{x}}(t), \mathbf{u}(t)) = 0 \\ & \mathbf{x}(0) + VT\mathbf{e}_\text{x} - \mathbf{x}(T) = 0, \end{aligned} \tag{8}$$

with the cost function $J(\mathbf{x}(t),\mathbf{u}(t))$ and the constraints on lower and upper bounds of $\mathbf{x}$ and $\mathbf{u}$ (see Appendix B), the dynamic equilibrium (Eq. 2) and periodicity with a forward translation in direction $\mathbf{e}_\text{x}$, where T was known[1] and the model's speed $V = \left(p^G_{x,\text{trunk}}(T) - p^G_{x,\text{trunk}}(0)\right)/T$ was unknown. The optimization problem was solved using direct collocation. Therefore, the state and control vectors were discretized at N collocation nodes using backward Euler

[1] We computed T from the average number of measurement points over multiple strides divided by the sampling frequency of the IMUs.

discretization. The cost function comprised a tracking term J_{track}, an effort term J_{effort} and a regularization term J_{reg}:

$$J = J_{\text{track}} + J_{\text{effort}} + J_{\text{reg}}. \tag{9}$$

In the tracking term, the squared difference between simulated signals (gyroscope: Eqs. 3-6, accelerometer: Eq. 7) and corresponding measured signals was minimized. For this, we computed the mean μ of measured sensor signals over multiple strides (see Sec. 2.4.3). We normalized the differences to the measured standard deviation of multiple strides σ to ensure that non-reproducible features such as noise and movement artifacts were not tracked:

$$J_{\text{track}} = \frac{1}{|\mathscr{S}|N} \sum_{k=1}^{N} \sum_{s \in \mathscr{S}} \left(\left(\frac{a_{\text{x},sk} - \mu_{a_{\text{x},sk}}}{\sigma_{a_{\text{x},sk}}} \right)^2 + \left(\frac{a_{\text{y},sk} - \mu_{a_{\text{y},sk}}}{\sigma_{a_{\text{y},sk}}} \right)^2 + \left(\frac{\omega_{sk} - \mu_{\omega_{sk}}}{\sigma_{\omega_{sk}}} \right)^2 \right). \tag{10}$$

In this work, we tracked sagittal inertial signals of seven inertial sensors, one placed at each segment of the musculoskeletal model. However, it is also possible to reduce the number of sensors and, for example, track only signals of foot-mounted sensors. In the effort term, we minimized the squared excitations of all 16 muscles to resolve muscle redundancy and to prevent the model from tracking noisy measurements, which would require high muscular effort:

$$J_{\text{effort}} = \frac{W_{\text{effort}}}{16NV^2} \sum_{k=1}^{N} \sum_{m=1}^{16} u_{mk}^2, \tag{11}$$

where W_{effort} is a weighting factor. Eq. 11 is similar to one used in previous work (van den Bogert et al., 2011), but we normalized the term with the squared speed of the model V^2. This was necessary to balance the tracking and effort terms when muscle activity increases over a wide range of walking and running speeds. We chose a quadratic normalization as previous work showed that muscle activity scales linearly with speed for walking and running (Belli et al., 1999; Neptune et al., 2008). The weighting was set empirically to $W_{\text{effort}} = 300$ testing $W_{\text{effort}} \in \{1, 100, 200, 300, 400, 500, 1000\}$. J_{reg} helped the convergence of the optimization and reduced the number of iterations by approximately 10%. It was proportional to the integral of the sum of squares of the time derivatives of all state and control variables. We kept J_{reg} small ($W_{\text{reg}} = 1e-5$) so that the result of the optimization was not influenced. The large-scale nonlinear optimization problem of Eq. 8 was solved using IPOPT (Wächter and Biegler, 2006). As initial guess, we used a simulation of walking ($1.4\,\mathrm{m\,s^{-1}}$) and running ($3.6\,\mathrm{m\,s^{-1}}$) generated by tracking optical motion capture data from independent data sets.

2.4. Evaluation Study

2.4.1. Study Design

We conducted a study evaluating our inertial motion capturing (IMC) analysis against a gold-standard optical motion capturing (OMC) analysis. We used seven custom-built IMUs (Portabiles GmbH, Erlangen, DE) (Blank et al.,

2014) including tri-axial accelerometers ($\pm 16\,\mathrm{g}$) and gyroscopes ($\pm 2000\,\mathrm{deg/s}$) sampled at 1000 Hz. The OMC system consisted of 16 infrared cameras (Vicon MX, Oxford, UK) and one force plate (Kistler Instruments Corp, Winterhur, CH), which were sampled at 200 Hz and 1000 Hz, respectively. These systems were synchronized using a wireless flash trigger, which was received by every IMU and fed back to an analog channel of the OMC system (Kugler et al., 2012). A trigger signal was either sent manually or when the subjects crossed a light barrier which started the OMC recording.

In total, ten healthy male subjects volunteered for the study (age: $27.1 \pm 2.6\,\mathrm{years}$; height: $1.82 \pm 0.05\,\mathrm{m}$; weight: $76.9 \pm 8.6\,\mathrm{kg}$). Ethical approval for data collection was given and informed consent was obtained from all subjects before the study. We fixed seven IMUs on the subjects' bodies: at the lower back, right and left lateral thigh, lateral shank, and upper midfoot. The position of the IMUs was measured with respect to the segments' coordinate systems as required to compute simulated accelerometer signals in Eq. 7. In addition, we placed 32 infrared reflecting markers at anatomical landmarks.

At the beginning of the data acquisition, we asked the subjects to perform different movements in the sagittal-plane for estimating the orientation of the sensors with respect to the segments' coordinate systems (see Sec. 2.4.3). The trigger was activated before every movement, which were: standing, bending the torso forwards and backwards, lifting the straight leg up and down and flexing and extending the foot. In addition, a T-Pose, in which the subject stood still with arms stretched out to the sides, was recorded for a static calibration of the OMC system. The subjects were told to walk and run at six speed ranges: $0.9\,\mathrm{ms^{-1}}$ to $1.0\,\mathrm{ms^{-1}}$ (slow walking), $1.2\,\mathrm{ms^{-1}}$ to $1.4\,\mathrm{ms^{-1}}$ (normal walking), $1.8\,\mathrm{ms^{-1}}$ to $2\,\mathrm{ms^{-1}}$ (fast walking), $3.0\,\mathrm{ms^{-1}}$ to $3.3\,\mathrm{ms^{-1}}$ (slow running), $3.9\,\mathrm{ms^{-1}}$ to $4.1\,\mathrm{ms^{-1}}$ (normal running) and $4.7\,\mathrm{ms^{-1}}$ to $4.9\,\mathrm{ms^{-1}}$ (fast running). The subjects had to perform ten valid trials each, i.e., the speed range was controlled using the light barrier and the force plate had to be hit with the right foot.

2.4.2. OMC Data Processing

We filtered the marker and force plate data using a second-order forward-backward low-pass Butterworth filter with a cut-off frequency of 10 Hz as suggested by Kristianslund et al. (2012). Afterwards, we downsampled the force plate data to 200 Hz and computed inverse kinematics and kinetics using the GaitAnalysisToolkit[2] which implements the methods of Winter (2009). Then, computed joint angles, moments and GRFs were segmented into individual gait cycles and the step on the force plate was identified as first step after the trigger signal. We extracted the walking trials from right heel strike to right heel strike according to the minimum of the right heel marker. The running trials were cut from left toe-off to left toe-off using the method of Handsaker et al. (2016). We had to differentiate between walking and running to ensure that the gait cycle was completely captured by the infrared cameras and the stance phase on the force plate was completely included. However, this did not affect the analysis as the same time section was used

[2] https://github.com/csu-hmc/GaitAnalysisToolKit

for OMC and IMC analysis. The joint angles, joint moments and GRFs of the ten trials at each speed were linearly interpolated to the same length and averaged afterwards. Finally, we decimated the mean and variance to 100 sample points by linear interpolation for comparison to the IMC analysis.

2.4.3. IMC Data Processing

First, the axes of the IMU sensors were aligned with the segmental coordinate systems of the musculoskeletal model using the functional calibration movements (Ferraris et al., 1995). Afterwards, we extracted the strides that were recorded by the OMC system. The IMU data was cut using the detected start and end of the gait cycle (see 2.4.2) relative to the trigger signal. The ten trials of each speed were linearly interpolated to the same length and averaged afterwards. Finally, we decimated the mean and variance to $N = 100$ sample points by linear interpolation for tracking the data with the musculoskeletal model (see Eq. 10).

2.4.4. Data Analysis

We computed the Pearson Correlation Coefficient (ρ) between the estimated variables of the OMC and IMC analysis using all time points (from all subjects and speeds). Thus, no assumption on the distributions of the coefficients had to be made. In addition, we correlated gait cycles individually and took the mean using Fisher's z-transform for comparing our results to Karatsidis et al. (2018). Here, we analyzed joint angles over the whole gait cycle and joint moments and GRFs over the stance phase. We categorized the correlation coefficients following Taylor (1990) into "weak" ($\rho \leq 0.35$), "moderate" ($0.35 < \rho < 0.67$), "strong" ($0.67 < \rho < 0.90$), and "excellent" ($\rho \geq 0.90$). In addition, we evaluated the absolute root-mean-square deviation (RMSD) of the joint angles, joint moments and GRFs in deg, in $\mathrm{BWBH\%}$[3] and $\mathrm{BW\%}$, respectively. The relative RMSD (rRMSD) was calculated as described in Ren et al. (2008). On the one hand, we used all samples and computed the RMSD applying ordinary least products (OLP) regression (Ludbrook, 1997). This removed the systematic error between the OMC and IMC method. On the other hand, we computed the RMSD and rRMSD without OLP regression for every single gait cycle individually and took the mean afterwards for comparison to Karatsidis et al. (2018).

3. Results

In total, 60 optimizations (ten subjects at six speeds) were solved with a mean CPU time of $50 \pm 26\,\mathrm{min}$ on Intel Xeon processors E3-1240. In the optimization, we tracked the data of seven IMUs with a musculoskeletal model. The resulting simulated IMU signals had the same overall curve shape as the measured signals, whereas the oscillatory parts after heel strike were not tracked (see Fig. 3). The optimizations yielded natural walking and running simulations (see videos in the supplementary material). Kinematics and kinetics were compared to the OMC analysis. Fig. 4 shows the

[3] in body weight (BW) and body height (BH)

results for one subject. All individual results including muscle activations and forces can be found in the supplementary material.

Fig. 5 shows the correlation between OMC and IMC analysis based on all subjects and speeds. Gait kinematics yielded excellent correlations and gait kinetics ($\rho \geq 0.93$) yielded strong to excellent correlation ($\rho \geq 0.90$). In addition, Table 1 provides a comparison to Karatsidis et al. (2018) as described in Sec. 2.4.4.

4. Discussion

In this work, we presented a novel approach to estimate gait kinematics, kinetics and muscle forces by tracking IMU data with a trajectory optimization. This method addresses the two major challenges of IMC mentioned in the introduction (see Sec. 1), low-quality data and incomplete measurements.

We tracked raw sensor data without integrating the signals. Integration drift was avoided by using periodic boundary conditions and the physics of frictional contact to constrain translational movements. Moreover, Fig. 3 shows that movement artefacts in the IMU signals after heel strike were not tracked whereas features with a low standard deviation were tracked well (see for example the longitudinal shank acceleration). This is because we normalized the tracking term by data variance (see Eq. 10), a model was used to eliminate solutions that are not dynamically consistent, and muscular effort was minimized (see Eq. 11).

We estimated gait kinematics, kinetics, and muscle forces solely based on IMU data without ground reaction force data. Ground reaction forces (GRF) were indirectly estimated via a combination of a contact model, and the GRF-induced acceleration signals. The method would even allow fewer IMU sensors to be used. In preliminary work, we were able to reconstruct gait using only IMU data of foot-mounted sensors. However, results were worse and we would suggest to track additional variables such as normal joint angles and GRFs from the literature, to avoid unrealistic solutions which are still consistent with a subject's foot IMU data.

Results of the trajectory optimization were robust with respect to the weighting of the effort term in the cost function (Eq. 11). For lower W_{effort}, joint angles improved slightly, whereas the resulting joint moments and GRFs got slightly worse. For higher W_{effort}, it was the other way round. Muscle activations were more noisy for lower W_{effort}, leading to noisy muscle forces. The normalization to squared speed allowed the same W_{effort} to be used for all speeds, reducing the need for tuning of the cost function. In future work, other effort measures could be used, such as metabolic cost (Koelewijn et al., 2018). Another possibility would be to learn the objective function from data (Clever et al., 2016).

The musculoskeletal model had several limitations that are relevant to the results of the study. The two-dimensional model limited the analysis to sagittal plane variables and muscles, but also may have affected the ability of the model to track IMU data. For instance, the model does not account for the effect of frontal plane rotation of the pelvis on the vertical accelerometer signal of the lower back IMU sensor. Our method can be used in a full 3D model to overcome

these limitations, albeit at the expense of longer computation time to solve the trajectory optimization problem. The musculoskeletal model had a rigid foot, which seems to have affected the running results. During running, the ankle plantarflexion moment rose too quickly, compared to the OMC results. We believe that the IMU on the upper mid-foot picked up an anterior pitch rotation, which the contact model then interpreted as an anterior shift in the center of pressure. A model with a deformable foot may have prevented this error. Similarly, the pelvis and upper body were represented by one rigid segment. The lower back IMU was placed on the sacrum and likely not representative of upper body dynamics, resulting in poor estimates of hip angle and moment. This error could be reduced by tracking additional upper body IMU sensors, possibly even without additional kinematic degrees of freedom. Another fundamental limitation is that the trajectory optimization approach uses a minimal effort criterion to distribute the effort among the muscles that actuate the joints. Unequal load distribution, and "unnecessary" antagonistic co-contraction will likely be missed. Integrating EMG sensing with IMU sensing will be necessary to resolve this issue.

Fig. 5 shows how the IMC results correlate to conventional OMC results, across subjects, across walking/running conditions, and across time points in the gait cycle. The overall correlation coefficients are all above 0.9, indicating that 80% of the true variance is predicted by the IMC analysis. Some gait cycles from the running tests seem to be outliers in the correlation diagram, and we suspect that these are local minima of their respective trajectory optimization problems. This could be alleviated by solving with multiple initial guesses, rather than one. The RMS differences between IMC and OMC are small enough for clinical applications where changes of 5-10 degrees in joint angle are clinically relevant (Khouri and Desailly, 2013). We suspect, however, that the correlations and RMS errors will be better for typical clinical study designs, where we are interested in differences between subjects (e.g. patient vs. normal) and even more so to determine within-subject changes such as treatment effects.

Compared to Karatsidis et al. (2018), we achieved similar performance (see Table 1) while reducing the number of software tools and processing steps. Our approach does not require a separate kinematic and kinetic analysis, combining the two into a single dynamic trajectory optimization. This has the advantage that no error propagation occurs and a dynamically consistent simulation is obtained. Thus, highly dynamic movements like running can be analyzed.

Similar to classical inverse dynamics, the IMU tracking approach has the limitation that individual muscle forces are resolved through an optimality criterion. In the present study, this is the effort term in the optimization objective. In pathological conditions where muscle force distribution is non-optimal (such as neurological disorders), muscle forces will be underestimated. In addition, any approach without force plate data will not uniquely resolve the load distribution between the two feet in a double support phase. This might affect clinical applications, such as stroke, where limb loads are not distributed optimally. Our validation study used able-bodied participants, so clinical validity is still an open question. In future work, the trajectory optimization approach can include EMG data in the tracking term of the optimization objective, in order to obtain solutions that are consistent with measured motion and EMG.

Trajectory optimization is fundamentally not a real-time analysis, because the optimization cannot start until data from an entire movement cycle has been collected. Higher computing power or larger convergence tolerances of the IPOPT would reduce computing time, and results may be available in near real time. On the other hand, three-dimensional models will eventually be needed which would likely increase the computation time dramatically.

In conclusion, gait kinematics and kinetics could be estimated for a wide range of speeds and subjects. We tracked inertial sensor data with a musculoskeletal model by solving an optimal control problem and obtained a dynamically consistent simulation. The method suppresses sensor artifacts and is drift-free. It provides a comprehensive gait analysis solely based on IMU data with a single software tool.

Conflict of Interest Statement

None of the authors had any financial or personal conflict of interest with regard to this work.

Acknowledgement

The authors thank Iris Kellermann for preliminary work and Heiko Schlarb for supporting the data acquisition. This research was supported by the Bavarian Ministry of Economic Affairs, Regional Development and Energy within the Embedded Systems Initiative. Bjoern Eskofier gratefully acknowledges the support of the German Research Foundation (DFG) within the framework of the Heisenberg professorship program (grant number ES 434/8-1).

Appendix A

This appendix provides details on the system dynamics in Eq. 2.

Contact Dynamics

We modeled foot-ground interaction with discrete contact points placed at $\mathbf{c}_0^{B_{\text{foot}}}$ in foot coordinate system B_{foot}. $\mathbf{c}_0^{B_{\text{foot}}}$ was the resting position without deformation. Each contact point was described with four state variables: the global position of the contact point $\mathbf{c}^G = \left[c_x^G, c_y^G\right]^T$ and the global force exerted by the ground on the contact point $\mathbf{F}^G = \left[F_x^G, F_y^G\right]^T$. The state variables can be expressed in foot coordinates using the transformation matrix $\mathbf{R}^{B_{\text{foot}}G}$:

$$\mathbf{c}^{B_{\text{foot}}} = \mathbf{R}^{B_{\text{foot}}G}\left(\mathbf{c}^{\text{G}} - \mathbf{c}^{\text{G}}_{B_{\text{foot}}}\right) \tag{12}$$

with the global coordinates of the foot origin $\mathbf{c}^{\text{G}}_{B_{\text{foot}}}$ and

$$\mathbf{F}^{B_{\text{foot}}} = \mathbf{R}^{B_{\text{foot}}G}\mathbf{F}^{\text{G}}. \tag{13}$$

The force-deformation properties were

$$\mathbf{F}^{B_{\text{foot}}} = k(\mathbf{c}^{B_{\text{foot}}} - \mathbf{c}_0^{B_{\text{foot}}}) + b\dot{\mathbf{c}}^{B_{\text{foot}}} \tag{14}$$

with the isotropic stiffness $k = 10^5 \mathrm{N\,m^{-1}}$ and isotropic damping $b = 100 \mathrm{N\,s\,m^{-1}}$.

Interaction between contact points and ground can be described as complementary problem. We would like to model hard contact, such that

$$F_y^G c_y^G = 0, \quad F_y^G \geq 0 \quad \text{and} \quad c_y^G \geq 0. \tag{15}$$

Eq. 15 states that the vertical force at a contact point F_y^G is zero unless the point is in contact with the ground and that contact points cannot penetrate the ground. In addition, we would like to have dry friction, such that

$$\dot{c}_x^G(F_x^G - \gamma F_y^G)(F_x^G + \gamma F_y^G) = 0, \quad \dot{c}_x^G F_x^G \leq 0 \quad \text{and} \quad -\gamma F_y^G \leq F_x^G \leq \gamma F_y^G, \tag{16}$$

with friction coefficient $\gamma = 1$. Eq. 16 states that the horizontal (friction) force F_x^G must be at the positive or negative limit when the point has a non-zero sliding velocity $\dot{c}_x^G$, that the F_x^G is opposite to the direction of sliding, and that the magnitude of F_x^G cannot exceed the friction limit, which is friction coefficient γ multiplied by the vertical force F_y^G. We converted Eq. 15 and Eq. 16 into nonlinear system of equations as introduced in Todorov (2010). We converted Eq. 15 into

$$F_y^G + s_y c_y^G - \sqrt{(F_y^G)^2 + s_y^2 (c_y^G)^2 + \lambda_y} = 0, \tag{17}$$

where $\lambda_y = 0.01$ is a small smoothing parameter chosen as compromise between accuracy and numerical efficiency and $s_y = 200$ is a scaling factor. Accordingly, we replaced Eq. 16 by a nonlinear equality:

$$\sqrt{(\gamma F_y^G (s_x \dot{c}_x^G - 1) - F_x^G)^2 + \lambda_x} - \sqrt{(\gamma F_y^G (s_x \dot{c}_x^G + 1) - F_x^G)^2 + \lambda_x} - 2F_x^G = 0, \tag{18}$$

where $\lambda_x = 0.001$ and $s_x = 10$. Eq. 17 and 18 were implicit constraints in the optimal control problem, as well as the subtraction of Eq. 13 and 14.

Equations of Motion

The equations of motion were derived with Kane's method using Autolev 4.1 (Symbolic Dynamics Inc., Sunnyvale, USA):

$$\mathbf{M}(\mathbf{q})\dot{\mathbf{v}} + \mathbf{B}(\mathbf{q}, \mathbf{v}) - \tau = \mathbf{0}, \tag{19}$$

where $\dot{\mathbf{v}}$ was approximated with finite differences, $\mathbf{M}$ is the mass matrix, τ the vector of generalized forces, and $\mathbf{B}(\mathbf{q}, \mathbf{v})$ contains gravity, centrifugal, coriolis effects and ground contact forces as a function of foot position and velocity.

Appendix B

This table summarizes the lower and upper bounds of the state and control variables used in the constrained optimal control problem in Eq. 8:

variable name	lower bound	upper bound
$p^G_{x,\text{trunk}}$	$-5\,\text{m}$	$7\,\text{m}$
$p^G_{y,\text{trunk}}$	$0.5\,\text{m}$	$2\,\text{m}$
$\theta_{\text{trunk}\|G}$	$-180\,\text{deg}$	$180\,\text{deg}$
$\theta_{\text{thigh\_r/l}\|\text{trunk}}$	$-90\,\text{deg}$	$160\,\text{deg}$
$\theta_{\text{shank\_r/l}\|\text{thigh\_r/l}}$	$-160\,\text{deg}$	$0\,\text{deg}$
$\theta_{\text{foot\_r}\|\text{shank\_r}}$	$-60\,\text{deg}$	$60\,\text{deg}$
$\mathbf{v}$	$-30\,\text{m/s}\|\,\text{deg/s}$	$30\,\text{m/s}\|\,\text{deg/s}$
$\mathbf{L_{CE}}$	$-1\,\mathbf{L_{CEopt}}$	$3\,\mathbf{L_{CEopt}}$
α	0	5
c^G_x	$-5\,\text{m}$	$7\,\text{m}$
c^G_y	$-0.5\,\text{m}$	$5\,\text{m}$
F^G_x	$-10\,\text{BW}$	$10\,\text{BW}$
F^G_y	$-0.5\,\text{BW}$	$10\,\text{BW}$
$\mathbf{u}$	0	5

References

Ancillao, A., Tedesco, S., Barton, J., O'Flynn, B., 2018. Indirect measurement of ground reaction forces and moments by means of wearable inertial sensors: A systematic review. Sensors 18 (8), 2564.

Belli, A., Kyrolainen, H., Komi, P. V., 1999. Changes in muscle activity patterns and kinetics. Strength And Conditioning 13 (4), 400–406.

Blank, P., Kugler, P., Eskofier, B. M., 2014. A wearable sensor system for sports and fitness applications. In Book of Abstracts of the 20th Annual Congress of the European College of Sport Science (ECSS). Amsterdam, The Netherlands, p. 703, available online: https://www5.informatik.uni-erlangen.de/Forschung/Publikationen/2014/Blank14-AWS.pdf.

Clever, D., Schemschat, R. M., Felis, M. L., Mombaur, K., 2016. Inverse optimal control based identification of optimality criteria in whole-body human walking on level ground. In Proceedings of the 6th IEEE International Conference on Biomedical Robotics and Biomechatronics (BioRob). University Town, Singapore, pp. 1192–1199.

Ferraris, F., Grimaldi, U., Parvis, M., 1995. Procedure for effortless in-field calibration of three-axis rate gyros and accelerometers. Sensors and Materials 7, 311–311.

Handsaker, J. C., Forrester, S. E., Folland, J. P., Black, M. I., Allen, S. J., 2016. A kinematic algorithm to identify gait events during running at different speeds and with different footstrike types. Journal of Biomechanics 49 (16), 4128–4133.

Hannink, J., Kautz, T., Pasluosta, C. F., Gaßmann, K.-G., Klucken, J., Eskofier, B. M., 2016. Sensor-based gait parameter extraction with deep convolutional neural networks. IEEE Journal of Biomedical and Health Informatics, 1–8.

Heinrich, D., van den Bogert, A. J., Nachbauer, W., 2014. Relationship between jump landing kinematics and peak ACL force during a jump in downhill skiing: A simulation study. Scandinavian Journal of Medicine and Science in Sports 24 (3), 180–187.

Karatsidis, A., Jung, M., Schepers, H. M., Bellusci, G., de Zee, M., Veltink, P. H., Andersen, M. S., 2018. Predicting kinetics using musculoskeletal modeling and inertial motion capture. arXiv preprint arXiv:1801.01668.

Khouri, N., Desailly, E., 2013. Rectus femoris transfer in multilevel surgery: technical details and gait outcome assessment in cerebral palsy patients. Orthopaedics & Traumatology: Surgery & Research 99 (3), 333–340.

Koelewijn, A. D., Dorschky, E., van den Bogert, A. J., 2018. A metabolic energy expenditure model with a continuous first derivative and its application to predictive simulations of gait. Computer Methods in Biomechanics and Biomedical Engineering 21 (8), 521–531.

Kok, M., Hol, J. D., Schön, T. B., 2014. An optimization-based approach to human body motion capture using inertial sensors. IFAC Proceedings Volumes 47 (3), 79–85.

Koning, B. H. W., van der Krogt, M. M., Baten, C. T. M., Koopman, B. F. J. M., 2013. Driving a musculoskeletal model with inertial and magnetic measurement units. Computer Methods in Biomechanics and Biomedical Engineering 18 (9), 1003–1013.

Kristianslund, E., Krosshaug, T., van den Bogert, A. J., 2012. Effect of low pass filtering on joint moments from inverse dynamics: implications for injury prevention. Journal of Biomechanics 45 (4), 666–671.

Kugler, P., Schlarb, H., Blinn, J., Picard, A., Eskofier, B., 2012. A wireless trigger for synchronization of wearable sensors to external systems during recording of human gait. In Proceedings of the 34th Annual International Conference of the IEEE Engineering in Medicine and Biology Society (EMBC). San Diego, California, USA, pp. 4537–4540.

Liedtke, C., Fokkenrood, S. A., Menger, J. T., van der Kooij, H., Veltink, P. H., 2007. Evaluation of instrumented shoes for ambulatory assessment of ground reaction forces. Gait and Posture 26 (1), 39–47.

Liu, T., Inoue, Y., Shibata, K., 2010. A wearable force plate system for the continuous measurement of triaxial ground reaction force in biomechanical applications. Measurement Science and Technology 21 (8).

Ludbrook, J., 1997. Special article comparing methods of measurement. Clinical and Experimental Pharmacology and Physiology 24 (2), 193–203.

Neptune, R. R., Sasaki, K., Kautz, S. A., 2008. The effect of walking speed on muscle function and mechanical energetics. Gait and Posture 28 (1), 135–143.

Prilutsky, B. I., Zatsiorsky, V. M., 2002. Optimization-based models of muscle coordination. Exercise and Sport Sciences Reviews 30 (1), 32–38.

Ren, L., Jones, R. K., Howard, D., 2008. Whole body inverse dynamics over a complete gait cycle based only on measured kinematics. Journal of Biomechanics 41 (12), 2750–2759.

Roetenberg, D., Luinge, H., Slycke, P., 2009. Xsens mvn: full 6dof human motion tracking using miniature inertial sensors. Xsens Motion Technologies BV, Tech. Rep 1.

Roetenberg, D., Luinge, H. J., Baten, C. T., Veltink, P. H., 2005. Compensation of magnetic disturbances improves inertial and magnetic sensing of human body segment orientation. IEEE Transactions on Neural Systems and Rehabilitation Engineering 13 (3), 395–405.

Sabatini, A. M., Ligorio, G., Mannini, A., 2015. Fourier-based integration of quasi-periodic gait accelerations for drift-free displacement estimation using inertial sensors. Biomedical Engineering Online 14 (1), 106.

Schepers, H., van Asseldonk, E., Buurke, J., Veltink, P., 2009. Ambulatory estimation of center of mass displacement during walking. IEEE Transactions on Biomedical Engineering 56 (4), 1189–1195.

Taylor, R., 1990. Interpretation of the correlation coefficient: a basic review. Journal of Diagnostic Medical Sonography 6 (1), 35–39.

Todorov, E., 2010. Implicit nonlinear complementarity: A new approach to contact dynamics. In Proceedings of the IEEE International Conference on Robotics and Automation (ICRA). Anchorage, Alaska, USA, pp. 2322–2329.

van den Bogert, A. J., Blana, D., Heinrich, D., 2011. Implicit methods for efficient musculoskeletal simulation and optimal control. Procedia IUTAM 2, 297–316.

van den Bogert, A. J., Read, L., Nigg, B. M., 1996. A method for inverse dynamic analysis using accelerometry. Journal of Biomechanics 29 (5), 667–671.

Wächter, A., Biegler, L. T., 2006. On the implementation of an interior-point filter line-search algorithm for large-scale nonlinear programming. Mathematical Programming 106 (1), 25–57.

Winter, D. A., 2009. Biomechanics and motor control of human movement. John Wiley & Sons.

Wouda, F. J., Giuberti, M., Bellusci, G., Maartens, E., Reenalda, J., van Beijnum, B. J. F., Veltink, P. H., 2018. Estimation of vertical ground reaction forces and sagittal knee kinematics during running using three inertial sensors. Frontiers in Physiology 9, 1–14.

Figures and Tables

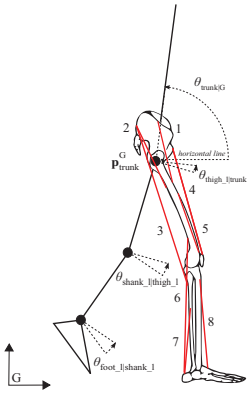

Figure 1: Musculoskeletal model with seven rigid segments and 16 Hill-type muscles: 1 - iliopsoas, 2 - glutei, 3 - hamstrings, 4 - rectus femoris, 5 - vasti, 6 - gastrocnemius, 7 - soleus, 8 - tibialis anterior. The model has nine kinematic degrees of freedom: The joint angles $(\theta_{\text{thigh\_l/r|trunk}}, \theta_{\text{shank\_l/r|thigh\_l/r}}, \theta_{\text{foot\_l/r|shank\_l/r}})$ and the global 2D position and sagittal orientation of the trunk $(\mathbf{p}^{G}_{\text{trunk}}, \theta_{\text{trunk}|G})$.

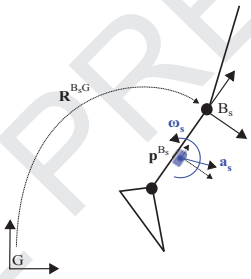

Figure 2: Virtual sensors are placed at position p^{B_s} in body-segment coordinate system B_s. Angular velocity ω_s and acceleration a_s are measured in B_s with respect to global frame G with the transformation matrix $R^{B_s G}$.

	Walking			Running			Walking (Karatsidis et al., 2018)		
	ρ	RMSD	rRMSD	ρ	RMSD	rRMSD	ρ	RMSD	rRMSD
Hip angle	1.00	8.2 (3.3)	21.9 (8.4)	0.98	8.7 (3.2)	16.5 (5.5)	0.99	5.7 (2.1)	12.7 (5.3)
Knee angle	1.00	5.5 (2.8)	8.8 (4.7)	0.99	5.3 (3.0)	6.1 (3.8)	0.99	4.4 (2.0)	7.2 (3.4)
Ankle angle	0.96	4.3 (1.5)	10.9 (3.4)	0.98	4.6 (1.7)	8.4 (3.8)	0.95	4.1 (1.3)	14.0 (4.8)
Hip moment	0.76	1.5 (0.4)	26.0 (9.8)	0.85	3.2 (1.0)	26.0 (6.8)	0.92	2.2 (0.6)	19.4 (4.2)
Knee moment	0.81	1.5 (0.4)	27.1 (9.2)	0.94	3.4 (1.2)	16.7 (7.1)	0.58	1.9 (0.5)	29.8 (7.6)
Ankle moment	0.95	1.6 (0.8)	14.4 (6.8)	0.96	3.2 (2.1)	17.1 (10.8)	0.93	1.6 (0.6)	15.1 (6.6)
A-P GRF	0.95	4.1 (1.2)	9.7 (2.1)	0.94	10.7 (3.9)	13.5 (4.2)	0.97	1.6 (0.6)	17.5 (6.8)
Vertical GRF	0.95	11.1 (3.4)	9.6 (2.5)	0.94	32.0 (7.9)	12.8 (3.6)	0.91	9.3 (3.0)	7.7 (2.1)

Table 1: Comparison of lower limb kinematics and kinetics between inertial motion capturing (IMC) and optical motion capturing (OMC): Mean Pearson Correlation Coefficient ρ, mean (standard deviation) of absolute and relative root-mean-squared differences, RMSD in deg, BWBH% and BW% and rRMSD in %, respectively.

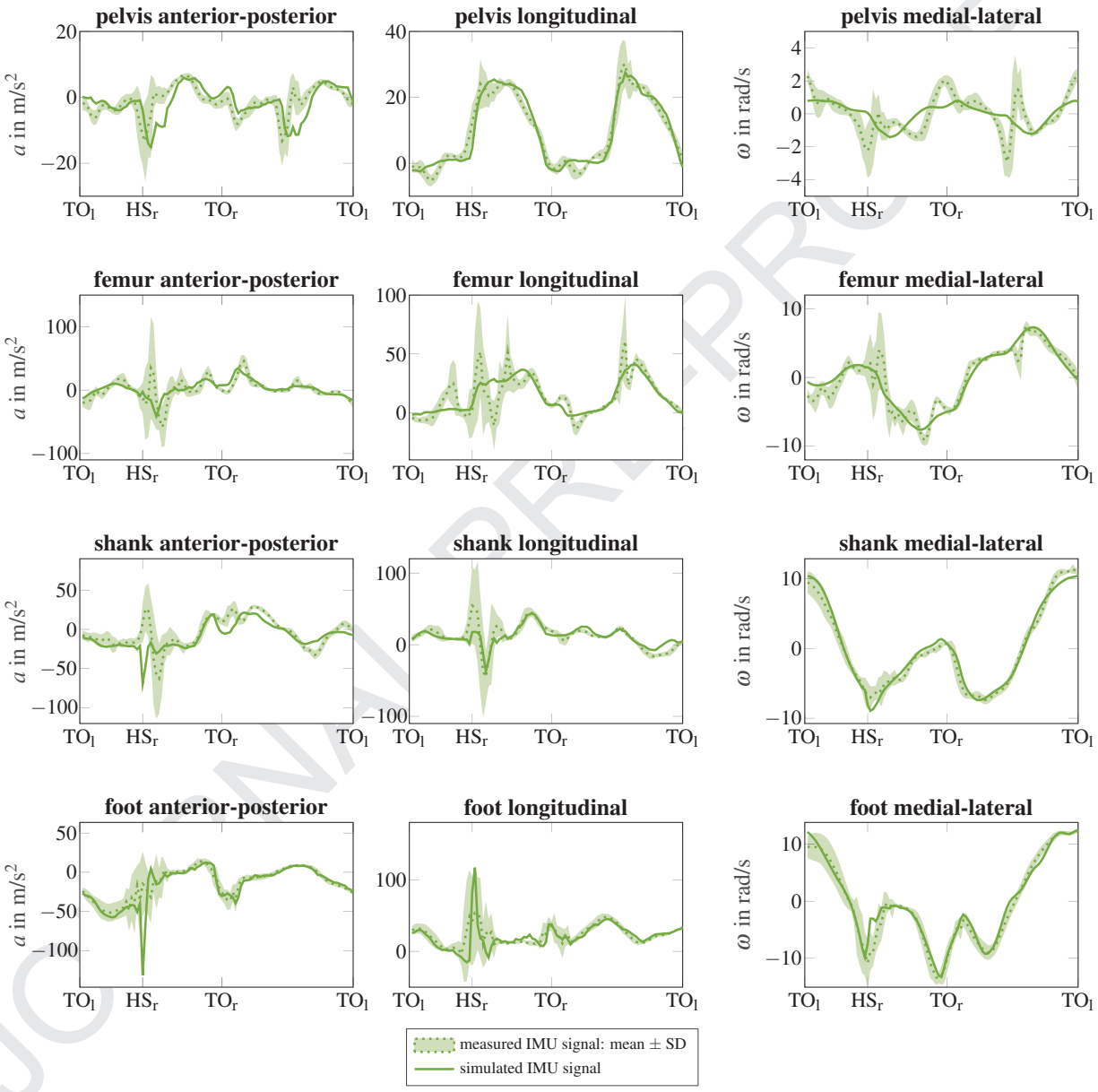

Figure 3: Measured and simulated inertial sensor data in the sagittal-plane of one subject running at normal speed. Mean and standard deviation (SD) of measured accelerations a and angular velocities ω (dotted line and shaded area) were tracked with a musculoskeletal model (solid line). Heel strike and toe off are denoted with HS and TO, respectively.

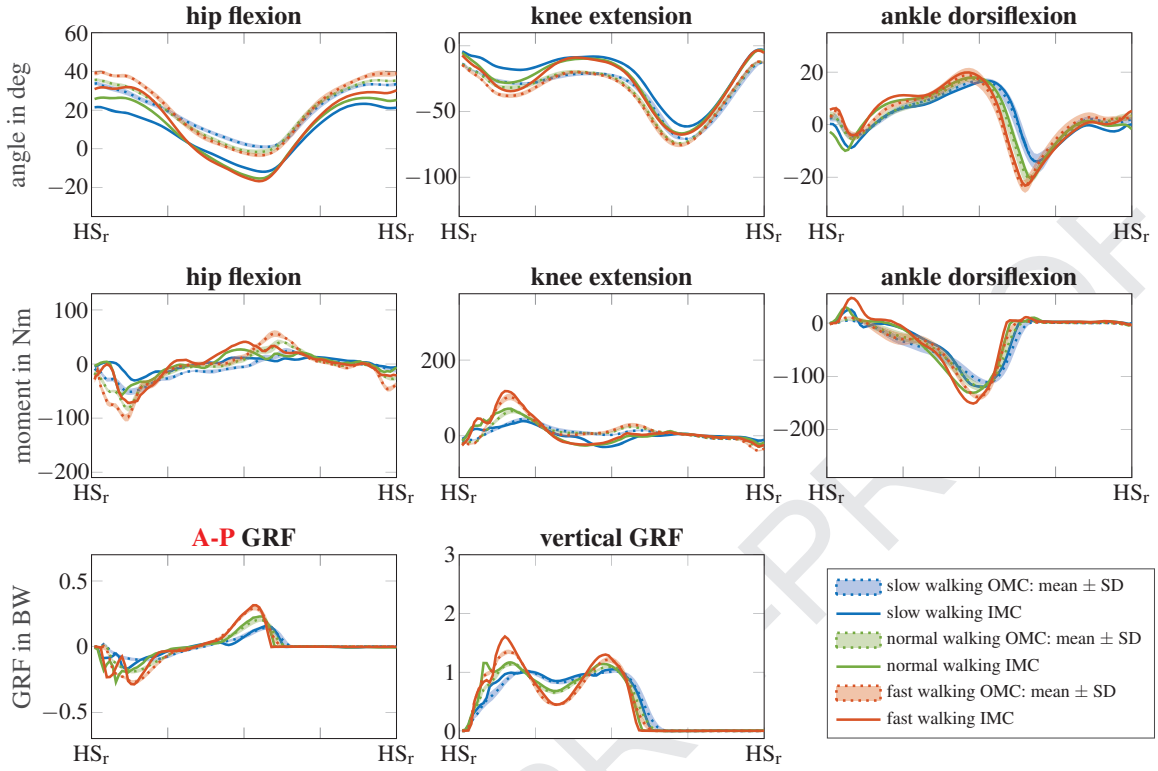

(a) Walking

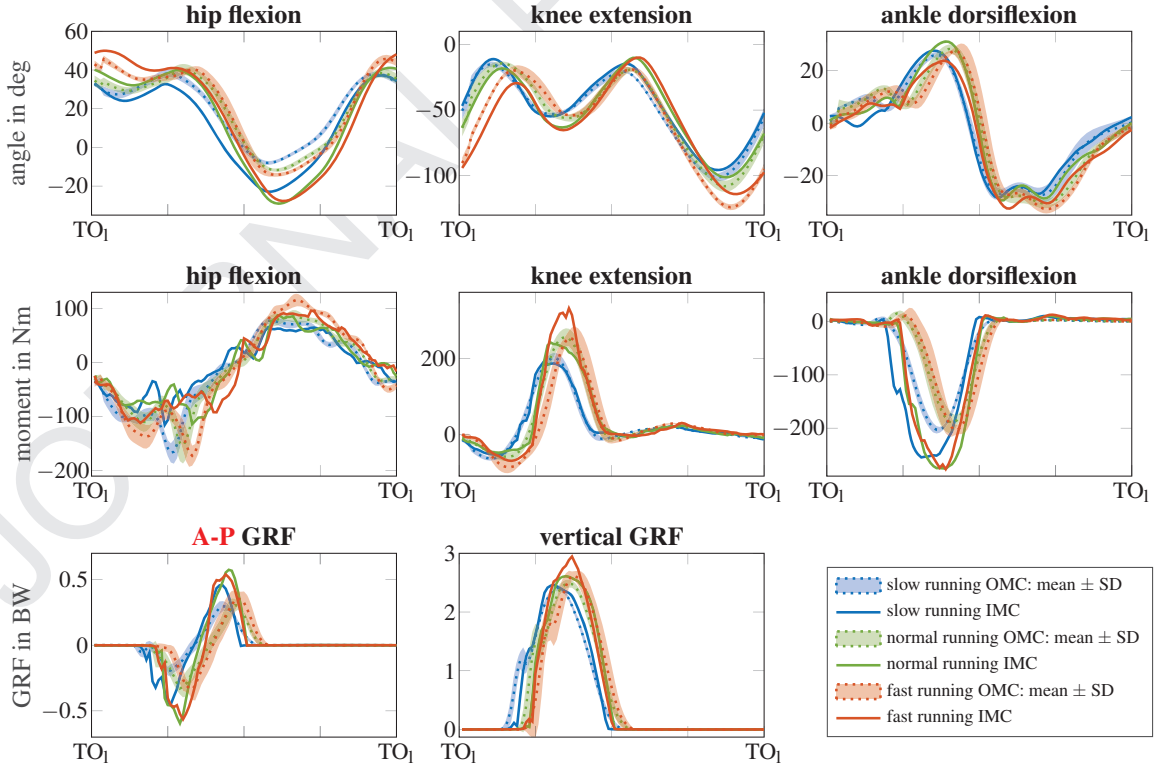

(b) Running

Figure 4: Lower limbs kinematics and kinetics in the sagittal-plane for one subject walking and running at slow, normal and fast speed: Comparison between inertial motion capturing (IMC) (solid line) and mean ± standard deviation (SD) of optical motion capturing (OMC) (dotted line and shaded area). Heel strike and toe off are denoted with HS and TO, respectively.

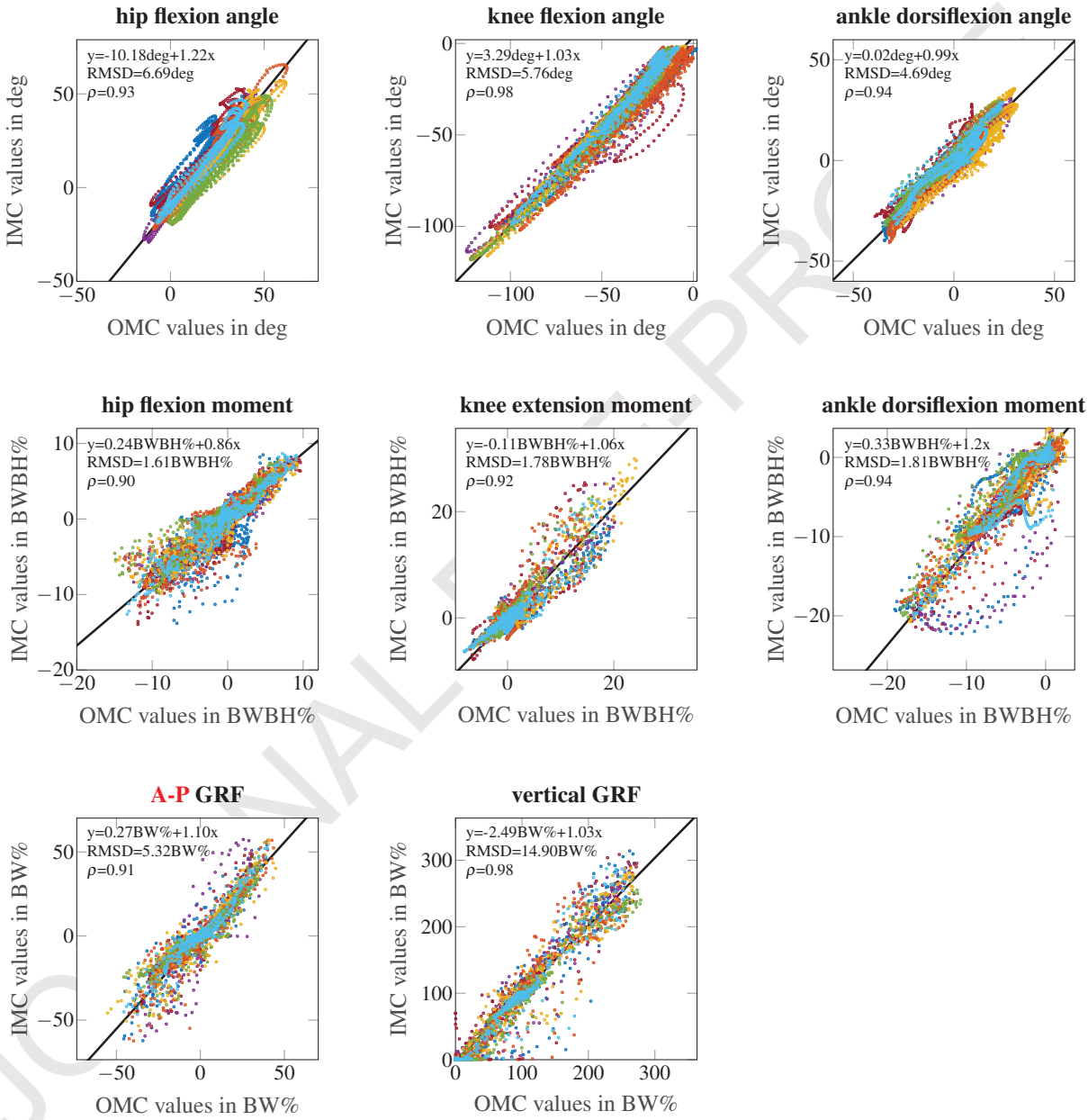

Figure 5: Lower limbs kinematics and kinetics in the sagittal-plane for ten subjects walking and running at slow, normal and fast speed: Correlation between inertial motion capturing (IMC) and mean of optical motion capturing (OMC) using ordinary least products regression for root-mean-square deviation (RMSD). Each correlation plot has 6000 data points, from 10 subjects, 6 movements, and 100 collocation points.